Effects of weld microstructure on static and impact performance of resistance spot welded joints in advanced high strength steels

M. I. Khan*, M. L. Kuntz and Y. Zhou

Evaluating the impact performance of resistance spot welded joints in advanced high strength steels (AHSS) is critical for their continued integration into the automotive architecture. The effect of strain rate on the joint strength and failure mode is an important consideration in the design of welded structures. Recent results suggest that the failure mode is dependent upon the strength, chemistry, and processing of AHSS. Current literature, however, does not explain the effects of weld microstructure and a comprehensive comparison has yet to be conducted. The present study details the fracture paths within the joint microstructure of spot welded AHSS, including dual phase (DP), transformation induced plasticity (TRIP) and ferritic–bainitic (FB), in comparison to new high strength low alloy steels. Quasi-static and impact tests were conducted using a universal tensile tester and an instrumented drop tower respectively. Results for elongation, failure load and energy absorption for each material are presented. Failure modes were detailed by observing weld fracture surfaces. In addition, cross-sections of partially fractured weldments were examined to detail fracture paths during static loading. Correlations between the fracture path and mechanical properties were developed using observed microstructures in the fusion zone and heat affected zone. Results showed that good impact performance was obtained in DP780 and TRIP780 grades in relation to DP600, 590R and conventional high strength low alloy.

Introduction

To meet goals of increased crash performance and occupant protection, automakers are replacing conventional mild steels with materials that have greater strength and good ductility. These materials include advanced high strength steels (AHSS), classified as group 3, with tensile strengths in the range 500–800 MPa. While AHSS show good ductility with elongation in the range 20–30%, the effects of welding on the crash performance are still a concern. The increased alloying levels required to give these materials higher strength results in an increase in hardenability during typical weld thermal cycles. Microstructures in the fusion and heat affected zone (HAZ) of resistance spot welds (RSW) are typically martensitic.[1] This hardened microstructure in the weld can lead to interfacial fracture during the high strain rates experienced in impact conditions, which is undesirable due to reduced elongation and energy absorption.[1] Furthermore, interfacial weld failures at low loads can adversely affect the load distribution, causing buckling and reducing energy absorbing crushing of structural members. Understanding the impact performance of spot welded AHSS is essential for the safe integration of these steels into the automotive architecture. Weld failure induced by impact loading rates is common to automotive applications; however, the mode of fracture can vary between different metallurgical types and grades of steel. The objective of the present work is to compare the effects of strain rate on failure in resistance spot welds for different types of group 3 AHSS, and detail the effects of fracture paths on the impact performance of spot welds.

The static and impact performance of spot welded high strength steels has been detailed in the literature.[2–5] Previous work has focused on group 2 steels with tensile strengths in the range 350–500 MPa. These materials typically exhibit good impact behaviour when spot welded. Ewing et al.[6] examined the tensile performance of RSW galvanised and bare high strength low alloy (HSLA) steels. Tests were conducted using velocities between $4 \cdot 5 \times 10^{-5}$ and $6 \cdot 7$ m s^{-1}. Results showed that the failure loads increased with test velocity for all weld schedules while the button failure modes remained consistent. In addition, it was shown that failure loads increased with base metal strength. Finally, it was observed that galvanising methods did not appear to have a statistically significant effect on the failure loads for the spot welded HSLA specimens.

Centre for Advanced Materials Joining, University of Waterloo, Canada

*Corresponding author, email Ibraheem@rogers.com

Currently, limited literature exists detailing the impact performance of spot welded AHSS material. Peterson and Orth[7] studied the influence of temperature and test velocity for spot welds on a single grade of 1·8 mm thick DP590. Test temperatures ranged from −75 to 400°C and test velocities from $1·3 \times 10^{-4}$ to 12·7 m s^{-1}. Results did not show a distinct transition temperature at the various loading rates; in addition, button failure modes were consistently produced. However, a slight increase in peak loads was observed at higher loading rates. It was shown that a reduction in absorbed energy at high test velocities was due to the reduction in material ductility in the weld microstructure.

The failure mode; however, is expected to vary between types of AHSS depending on alloying level and material processing. Thus, a comparative study which details the impact performance of spot welded AHSS is still required to support safety and design objectives. Furthermore, detailed analysis of fracture paths during loading remains to be examined and related to the weld microstructures. The present study details the impact performance of different metallurgical types of AHSS, including dual phase (DP), transformation induced plasticity (TRIP), and ferritic–bainitic (FB). High strain rate impact testing was conducted to emulate crash conditions experienced in automotive applications. The effects of testing rate on failure loads, energy absorption and elongation are detailed by examining the fracture surface and failure paths.

Experimental

Four different types and grades of group 3 AHSS were studied, including DP600, DP780, TRIP780 and 590R. An HSLA350 steel was also included to represent conventional group 2 high strength steels and benchmark AHSS performance. Table 1 shows the steel grades and chemical compositions for the materials used in the present study. Advanced high strength steels are typically classified by microstructural constituents and tensile strength. Chemistry ranges used in AHSS production can vary as per the manufacturer and manufacturing method. The multiphase microstructures are typically produced through cold rolling and annealing processes. Detailed processing routes are still proprietary to steel manufacturers, as such; they cannot be specified in the present work. However, referenced works provide information on the general production methods used in the creation of these materials.[8,9] In the included TRIP steel, Si is the dominant constituent aiding in the formation of retained austenite, however other TRIP steels exist using Al as an additive.

Spot welded samples were produced using a CenterLine (Windsor) Ltd 250-kVA pneumatically operated single phase RSW machine with constant

current control and a frequency of 60 Hz. An E-nose RWMA class 2 electrode with a 6·0 mm face diameter was used, according to AWS standards for the thickness range of the material tested in the present study.[10] Cooling water flowrate and hold time also followed AWS recommendation of 4 L min^{-1} and five cycles respectively. The RSW machine was fully equipped with a DAQ system capable of recording load, displacement ($\pm$0·01 mm), current and voltage simultaneously as a function of time. A linear transducer mounted to the top electrode measured the displacement while a calibrated coil collected the dI/dt, which was conditioned to obtain current as a function of time. A load cell located under the bottom electrode measured the force applied by the overhead cylinder. The data acquisition rate was 25 000 points per second. Additional information on data monitoring for the resistance spot welding process is described elsewhere.[11,12]

Optimal welding parameters were developed by examining failure loads via overlap tensile shear testing at the static test velocity. Table 2 shows the optimal welding parameters arrived at for each material. Optimisation testing was conducted to determine weld conditions which produced acceptable weld qualities as determined by AWS standards.[10] A full factorial technique was used to optimise welding parameters to attain maximum failure load. The weld current was varied from 7 to 10 kA, the weld force ranged from 3·5 to 5·5 kN, and the weld time was between 10 and 20 cycles for each material. The weld samples were subjected to overlap tensile shear testing, coach peel testing, and metallographic examination. During schedule optimisation, a total of 11 tests were conducted per condition including five tensile tests, five peel tests and one sample for metallographic preparation. One standard deviation was calculated for each dataset to determine error bar ranges.

Three test rates were selected for overlap shear testing, which included static ($8·3 \times 10^{-7}$ m s^{-1}), intermediate ($1·7 \times 10^{-3}$ m s^{-1}) and impact (5·36 m s^{-1}) test velocities. Static and intermediate test velocities were performed using a universal tensile testing machine. Measures were taken to maintain coplanar alignment

Table 2 Optimal welding parameters

	Welding parameter			Nugget diameter, mm
	Force, kN	Current, kA	Time, cycles	
HSLA	3·5	9	20	6
590R	5·5	9	20	5·9
DP600	3·5	8	20	5·4
DP780	5·5	9	15	6·4
TRIP 780	4·5	8	20	5·6

Table 1 Material properties

Steel grade	Thickness, mm	Coating		Alloying elements, wt-%				
		Type	Ave. wt, g m^{-2}	C	Mn	Mo	Cr	Si
HSLA	1·0	GI	73·9	0·060	0·640	0·010	0·050	0·240
590R	1·2	GA	43·4	0·130	1·599	0·013	0·029	0·120
DP600	1·2	HDGI	55·1	0·100	1·523	0·196	0·197	0·157
DP780	1·15	GA	58·8	0·113	2·082	0·181	0·239	0·036
TRIP780	1·0	HDGI	62·5	0·188	1·631	0·012	0·023	1·618
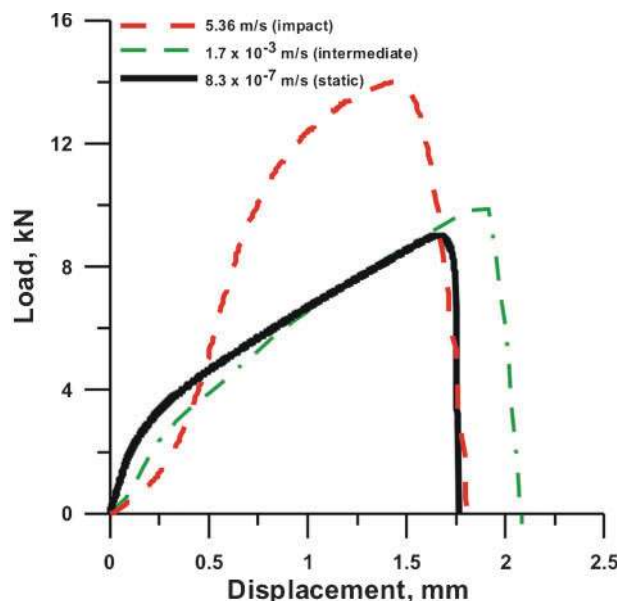
1 Representative load–displacement curve for DP600

during mechanical testing by using shims in the grips. Detailed examination of failure mechanisms was facilitated by interrupting the loading cycle during overlap shear testing at static strain rates.

Impact testing was conducted on an instrumented falling weight impact tester. Capabilities of the instrumented falling weight impact tester include compression, biaxial tension, toughness and uniaxial tension testing. Fixturing allowed for a coplanar geometry to be maintained without the use of shims. A load cell located above the upper grip monitored the force while a magnetic displacement sensor measured relative displacement. A total of five tests were conducted at each loading rate.

Figure 1 shows a representative load *v.* displacement curve for DP600 obtained for static, intermediate and impact test velocities. An energy trace for the static testing velocities is also plotted. Key parameters obtained from these curves include failure load, displacement at failure and energy absorbed. The amount of energy absorption was digitally calculated by measuring the area under the load–displacement curve up to failure[13] using the following equation

$$Q = \sum_{n=1}^{N} F(n) \cdot [x(n) - x(n-1)] \qquad (1)$$

where F is force, x the displacement, n the sampled data and N the peak failure load.

The materials used in the present study consisted of nominal thicknesses ranging from 1·0 to 1·2 mm. In addition, the weld size produced by the optimised schedule for maximum static tensile strength varied slightly. Table 2 shows the weld nugget diameter measured metallographically for the optimised condition in each type of AHSS. There was very little difference in the optimised weld sizes, which ranged from 5·4 to 6·4 mm. Since the process parameters were optimised for static tensile shear strength, the failure loads can be directly compared for each material. To account for the slight differences in sheet thickness and weld size, a normalisation approach was used to compare the failure loads and energy absorption for each material at

different test velocities. The following equation was used in normalising results

$$N = \frac{X}{\pi D \cdot t} \qquad (2)$$

where N is the normalised result, X normalising variable (failure load or elongation), D nugget diameter and t material thickness.

During metallographic examination all test sections were etched using Lepera's reagent to distinguish between the different phases in the fusion zone (FZ), HAZ and base metal (BM), When this particular etchant is used, martensite is etched white, α-ferrite is grey and bainite is black.

Results and discussion

Base metal microstructure

Base metal microstructures for the selected steels are shown in Figure 2. Fig. 2a shows the HSLA comprising of ferrite grains (grey) with carbides (dark coloured) situated at grain boundaries. The FB 590R, as shown in Fig. 2b, contains non-uniformly sized ferrite grains (grey) with grain boundary bainite (black). The DP600 and DP780, as shown in Fig. 2c and d respectively, consists of dispersed martensite islands (white) embedded in a ferrite matrix with the DP780 exhibiting a relatively higher volume fraction of martensite. The TRIP780, microstructure consists of retained austenite (white) and dispersed bainite (black) within a ferrite matrix (grey), as shown in Fig. 2e.

Load to failure

Figure 3 shows the relationship between failure loads and test velocities for static, intermediate and impact rates. General trends showed an increase in failure load with test velocity. Similar results have been reported by Ewing *et al.*[6] for spot welded HSLA. Failure loads increased between static to intermediate rates, however there is a notable drop in displacement when transitioning from intermediate to impact velocities. It has been shown that the increase in strain rates results in increased flow stress;[14] which in turn limits elongation of the material in the spot weld.[15,16] It has been speculated that this can increase the peak load of the weldment.[7] Thus, fracture could result at a higher peak load with lower overall elongation which can reduce the energy absorbed by the weld.

Normalised results, which account for material thickness and nugget diameter, are shown in Fig. 4. The TRIP780 steel exhibited the highest overall load bearing capacity for all three test velocities; followed by DP780 and 590R. During static and intermediate test velocities the DP600 and HSLA had similar load bearing capacities $\sim 0{\cdot}4$ kN mm^{-2}. However, impact failure loads for HSLA approached $0{\cdot}9$, outperforming DP600 and slightly surpassing DP780 and 590R. A direct correlation between base metal strength and failure loads was not clearly evident for spot welded AHSS. This is contrary to results observed by Ewing *et al.*[6] for HSLA that showed increased failure loads with base metal strength.

Sample elongation

Figure 5 shows the general trend of increasing sample elongation to failure with increasing test velocity from
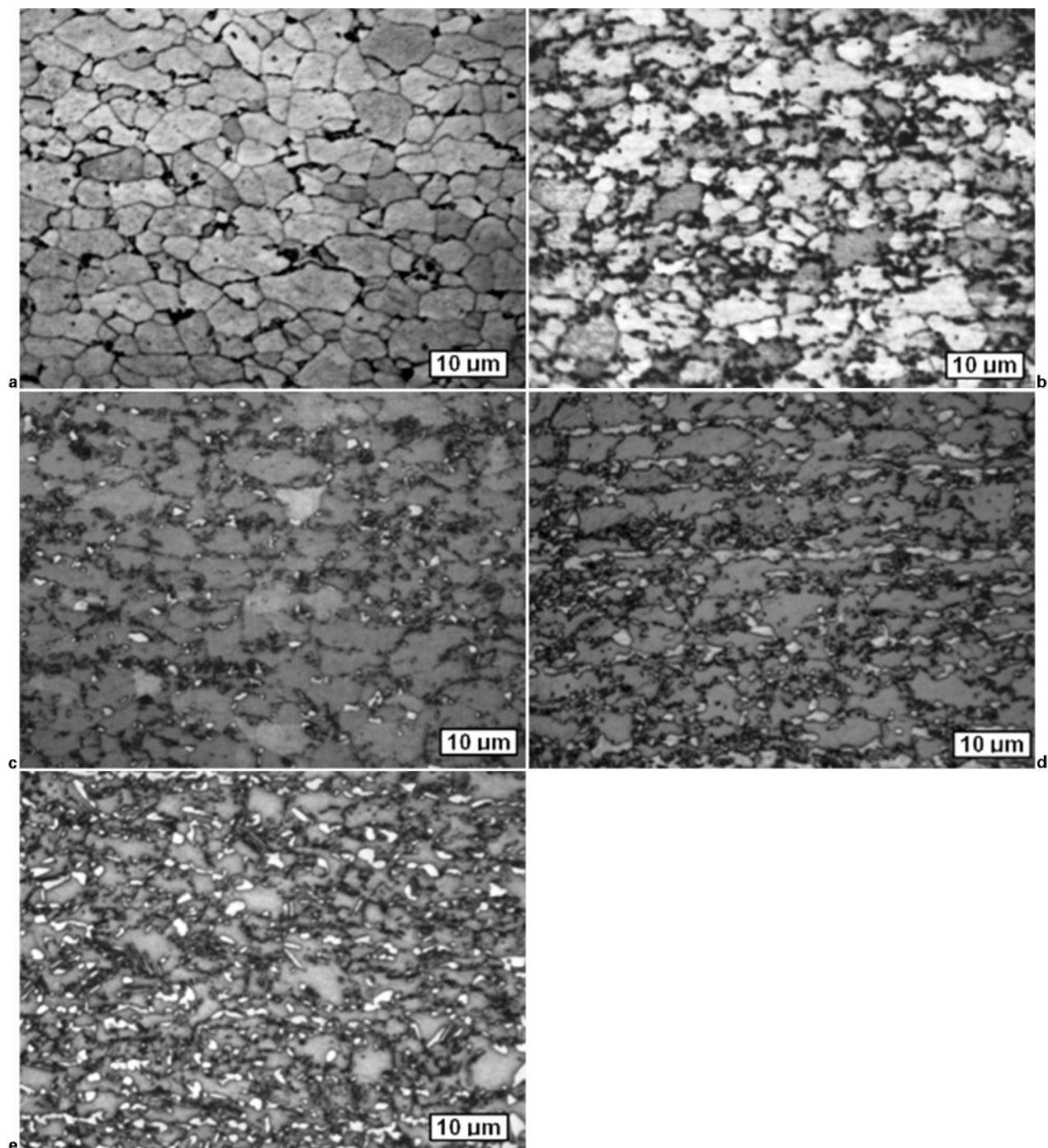
a HSLA; *b* 590R; *c* DP600; *d* DP780; *e* TRIP780
2 Base metal microstructure selected steels

static to intermediate, and then decreasing elongation from intermediate to impact velocities. At static conditions, the DP600 showed a significantly lower elongation than the other test materials, which exhibited similar performance. DP600 elongation was consistently low for all testing conditions. At the intermediate testing rate, TRIP780 showed the greatest change, with an increase of ~1 mm (25%). Elongation of the HSLA and 590R steels decreased considerably (50%) from intermediate to impact velocities. Materials with the highest base metal strength (DP780 and TRIP780) exhibited a notably higher RSW sample elongation at impact velocities. This is in contrast to the expected base metal performance which was expected to be higher for the HSLA and

lower strength materials, which typically exhibit greater ductility. The FB type 590R, which is designed to have greater elongation and better crash performance showed low elongation in RSW samples at impact velocities; however, reasons for this will be explained later in the present study.
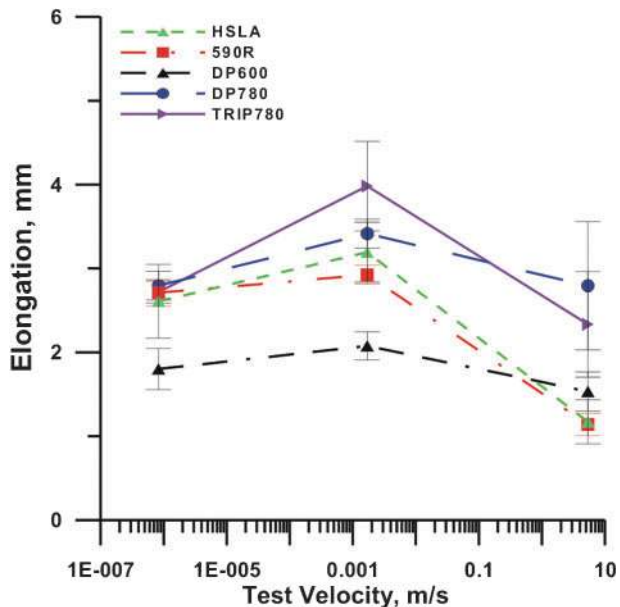
Energy absorption

Figure 6 shows the energy absorption for the RSW samples in each material at the three rates tested. General trends show an increase in absorbed energy from static to intermediate test velocities, followed by a decrease when transitioning from intermediate to impact rates. Normalisation of energy results, shown in Fig. 7, results in

3 Failure load *v.* test velocity
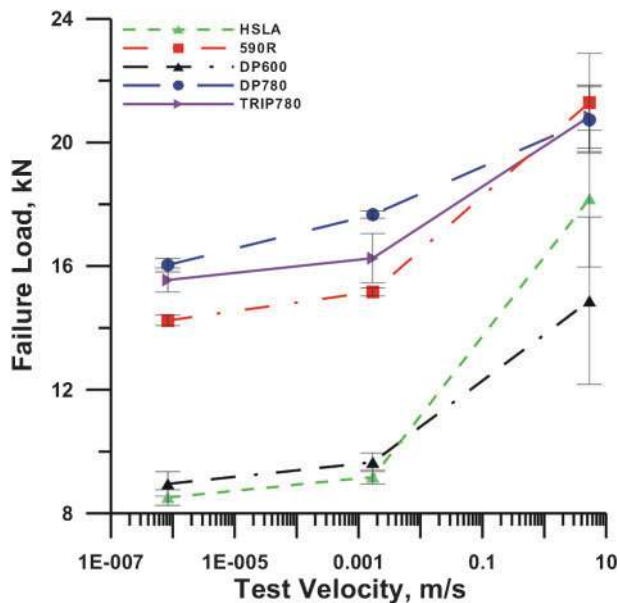

5 Elongation *v.* test velocity

slightly increased performance of TRIP780 relative to the other materials tested. The relationship between energy, failure load, and elongation described in equation (1) is manifested in this figure. Even though the peak failure loads generally increase with increased testing rate, the effect of reduced elongation at impact velocities dominates the energy absorption, resulting in a decrease in energy from intermediate to impact rates. The HSLA and 590R show a considerable reduction in energy, which is reflected in the elongation shown in Fig. 5. Both materials show similar results which were close to the poorly performing DP600. Conversely, TRIP780 showed the highest energy absorption value followed by DP780. The low energy absorption to failure load of 590R at the high test velocity is a function of the failure mode, this and the performance of the other materials can be explained by analysis of the spot weld fracture.
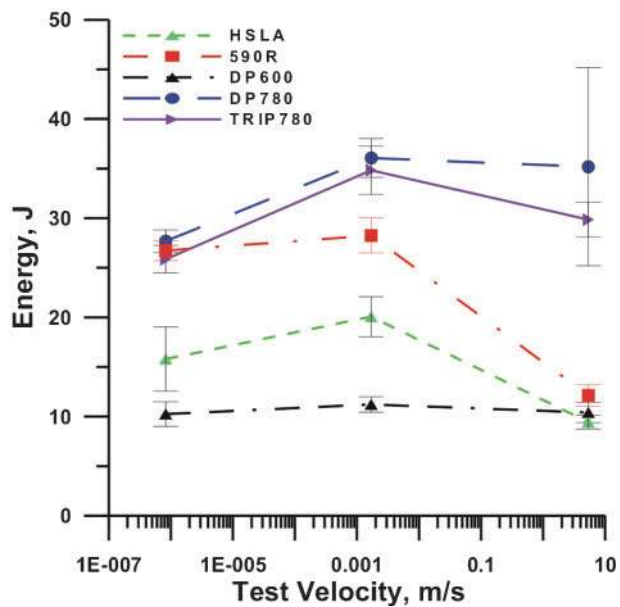
Failure mode

A schematic of the typical tensile failure modes and fracture paths are shown in Fig. 8. The three distinct fracture paths inherent to RSW tensile failure include interfacial (mode A), partial interfacial (mode B) and button pullout failure (mode C and D). Mode A shows the fracture path for interfacial failure in which fracture propagates through the fusion zone following the centreline structure, typically resulting in reduced elongation. During mode B failure, fracture propagates along the interface and redirects perpendicularly to the centreline towards the sheet surface, resulting in partial interfacial failure. Button pullout failure modes typically result when failure occurs at the outer edge of the HAZ. This can include fracture initiating along the HAZ/BM interface, mode C, or even failure occurring only in the base metal, mode D. The characterisation of these
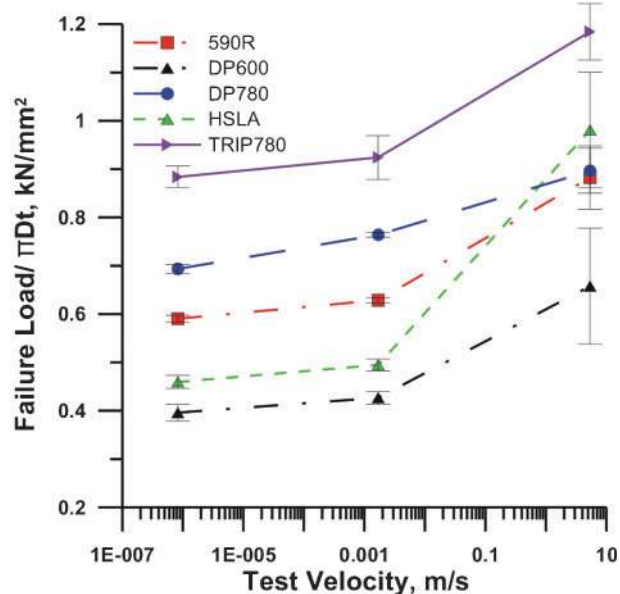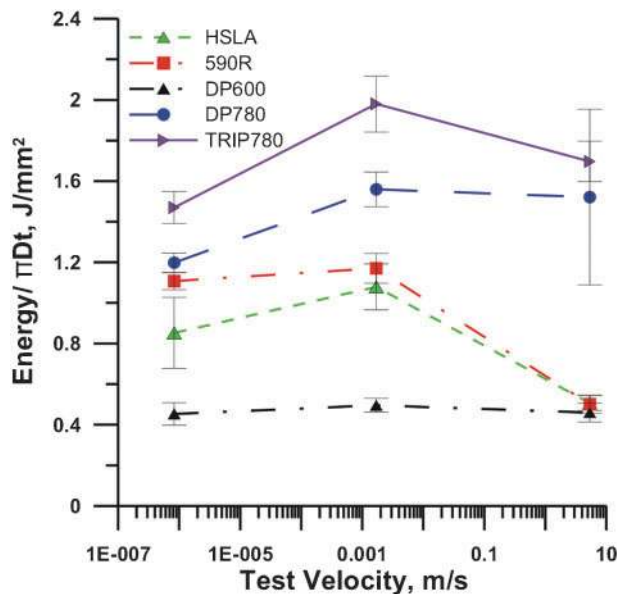

4 Normalised failure load *v.* test velocity
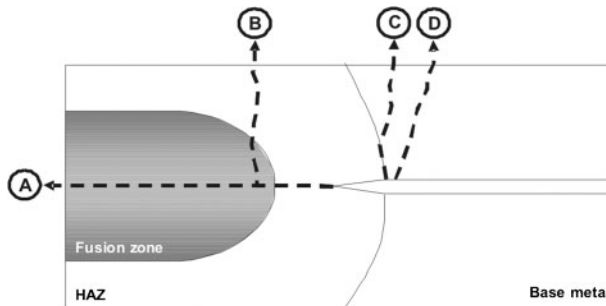

6 Absorbed energy *v.* test velocity

7 Normalised energy *v.* test velocity

**8 Schematic of weld joint cross-section with typical tensile shear failure modes**

failure modes will be used to describe the failure modes observed in the present study.

Figure 9*a–c* shows the fracture surfaces of spot welded DP600. Mode A failure can be observed for all three test velocities. In Fig. 9*d* the cross-section for the partial tensile sample tested at the static test condition is illustrated. Fracture initiated at the interface of the two materials and propagated through a narrow region of solid state bonding and into the FZ. Further loading would cause fracture to propagate through the FZ centreline, resulting in full interfacial failure. The FZ and HAZ near the fusion boundary consists of a fully martensitic structure. In addition, discontinuities along the centreline caused by solidification cracking have been reported in DP600 and can adversely affect the overall bonded area.[17] The poor fracture toughness of the martensitic structure along with the stress concentration at the interface resulted in low failure loads at all test velocities. Sample elongation of the DP600 was also very low compared with the other materials in the present study, resulting in low energy absorption for all conditions. The consistently poor results observed with DP600 could potentially be avoided with the use of pulsing. It has been shown that pulsing can be used for *in situ* heat treatment of the weld material.[12] This can
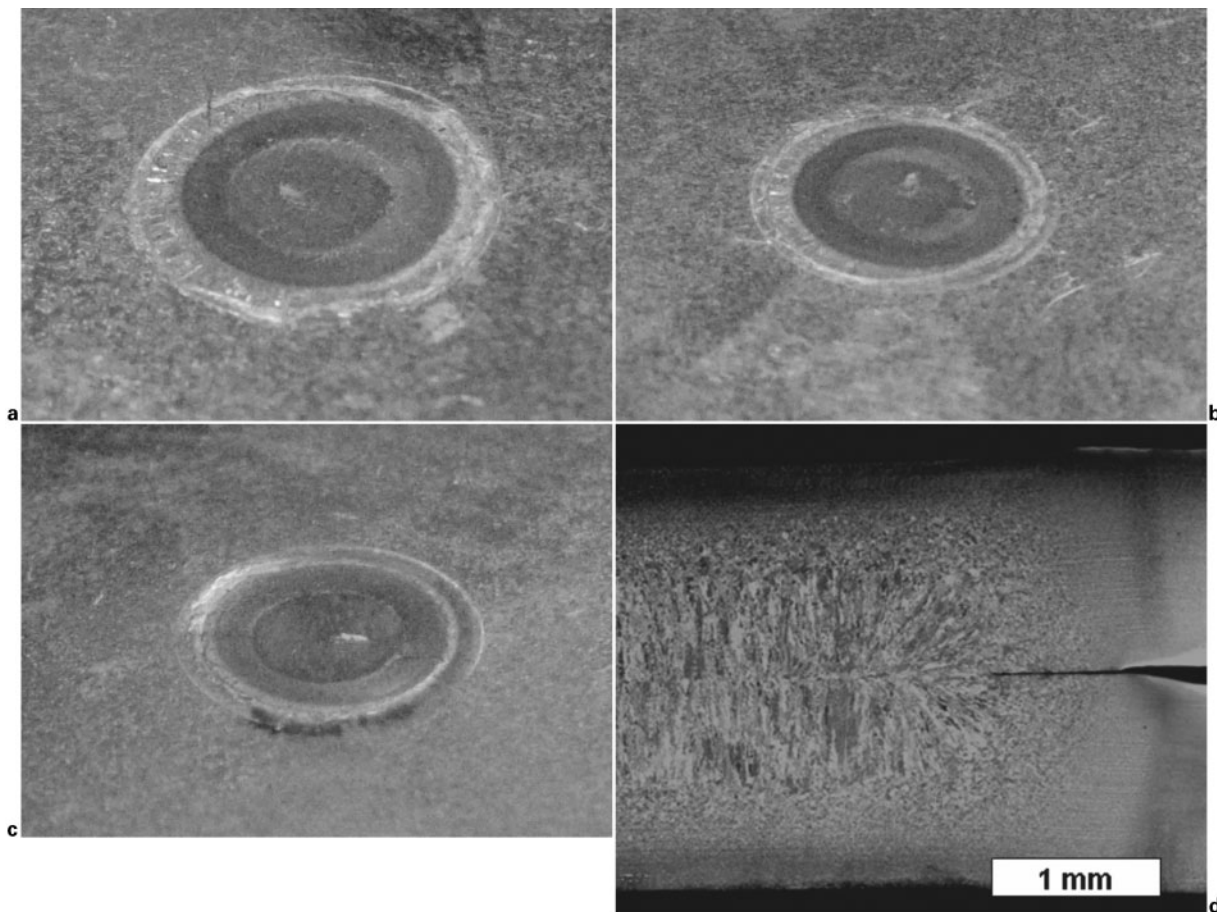
a static; *b* intermediate; *c* impact; *d* fracture cross-section
9 Typical fractured coupon appearance for DP600 material
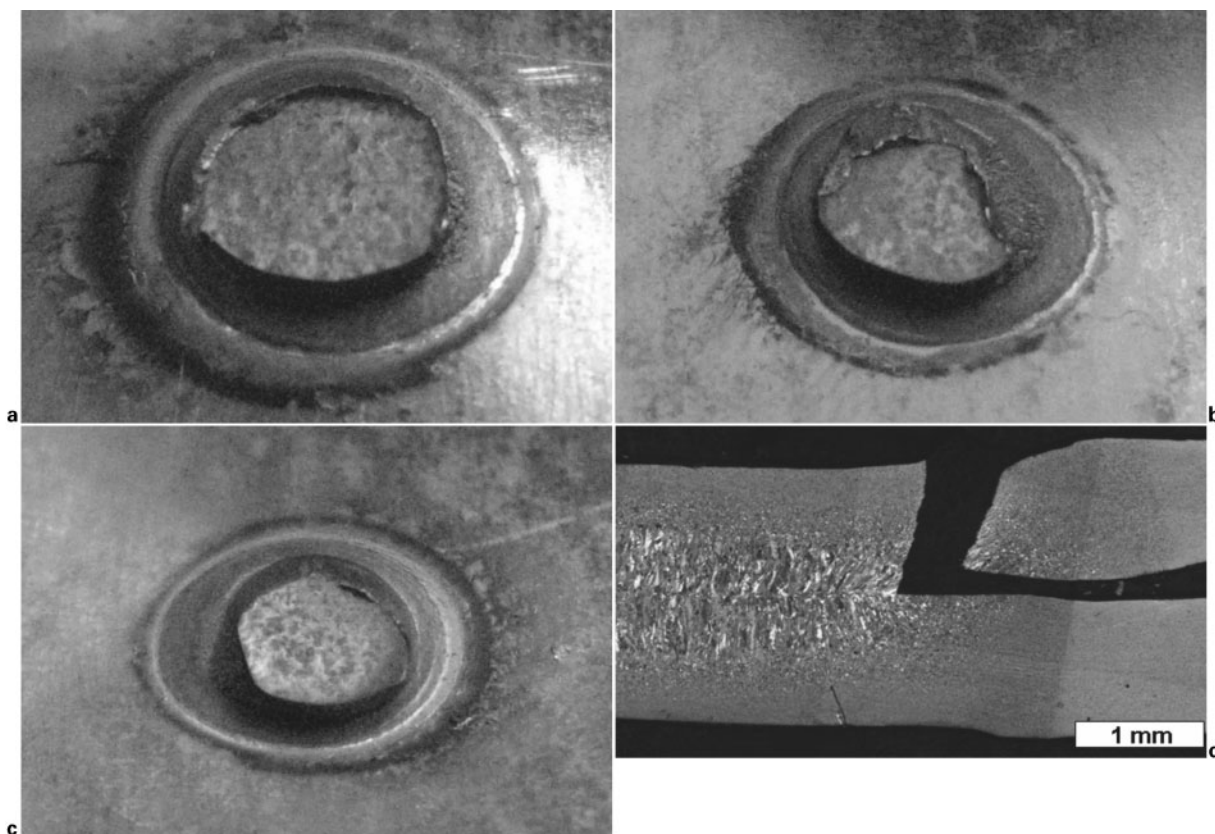
a static; *b* intermediate; *c* impact; *d* fracture cross-section
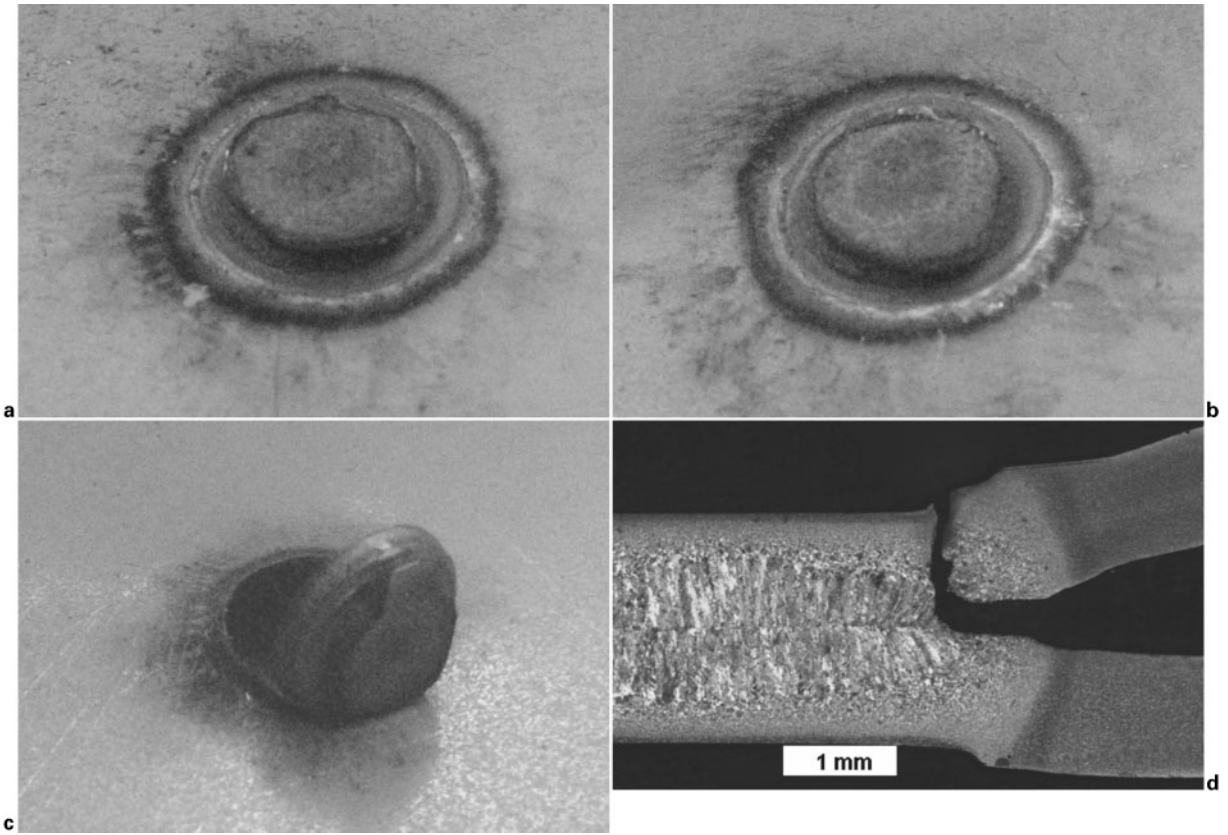**10 Typical fractured coupon appearance for HSLA material**

modify the microstructure within the weldments and potentially improve mechanical properties including impact performance. Other work[10] has shown that a transition from interfacial failure to a button pullout failure mode by increasing the weld size; however, this comes with a penalty of increased energy input and greater risk of overwelding and excessive expulsion.

Fracture surfaces for the spot welded HSLA at three test velocities are shown in Figure 10*a–c* for the static, intermediate and impact cases respectively. Partial interfacial failures, mode B, were observed for all three test velocities; however, the failure was nearly a button pullout. By observing the detached upper sheet, portions of the FZ can be seen, suggesting that fracture propagated through some of the FZ material. Figure 10*d* shows the cross-section for the static partial tensile test. From this, it is confirmed that fracture initiated at the interface of the two materials and started to propagate through the fusion zone before final through sheet fracture occurred in the HAZ. The base metal material showed little evidence of plastic deformation. The post-weld microstructure in the FZ and HAZ was mostly bainitic. The results for low, intermediate and high rate testing are consistent with what is found in the literature for HSLA materials. Typically, the failure load increases at higher velocities; however, the corresponding low elongation results in lower toughness than the other materials with higher strengths in the present study.

Fracture surfaces for the TRIP780 spot welds are shown in Fig. 11*a–c*. The failure mode in the TRIP steel for all test velocities is similar to mode B, which is also observed in the HSLA spot welds. Figure 11*d* shows the cross-section for the static partial tensile shear test.

Fracture initiates near the sheet interface and propagates towards the FZ before redirecting along a vertical dendrite boundary and failing through the sheet. It has been shown that rich chemistries inherent to TRIP780 production can result in segregation of alloying elements during weld solidification.[18] The segregated microstructure provides preferred paths for crack propagation within the FZ. Uijl *et al.*[18] suggested using a modified RSW schedule with a second welding pulse which can heat treat the weld metal, resulting in a more ductile button failure mode. In the present study, however, the TRIP steel demonstrated the highest failure loads at low, intermediate and high test velocities. This can be attributed to the high hardness of the martensitic structure in both the FZ and HAZ. Necking in the base metal is observed in the outer HAZ and base metal (Fig. 11*d*), which gives good elongation before final fracture and is also observed in the results. Transformation induced plasticity steels demonstrate steady strain hardening that persists over a wide range of strain.[19] Final fracture then occurs at the high hardness, high strength weld region. From the results, the TRIP steel demonstrated the highest toughness at all velocities.

Figure 12*a–c* shows the fracture surfaces of DP780 for all three test velocities. Button pull-out failure modes were observed during static and intermediate test velocities with remains from the HAZ material surrounding the FZ. However, during impact testing there was full separation of the nugget from the welded sheets. After each impact test three components would remain in the drop chamber including the two welded coupons and a fully separated nugget. By examining the cross-section of the partial tensile sample, Fig. 12*d*, it can be

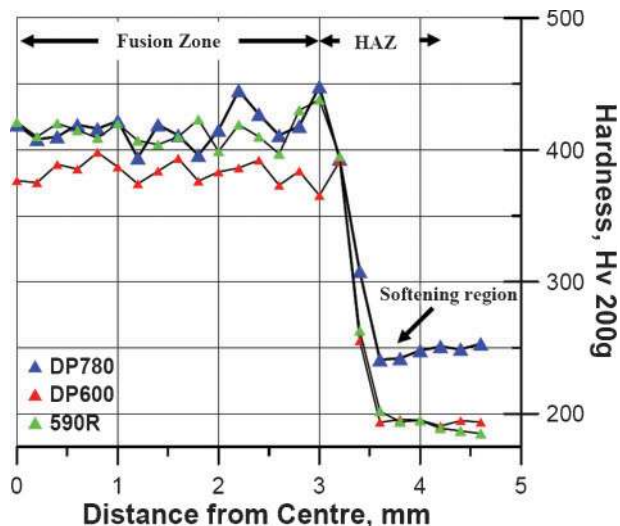*a* static; *b* intermediate; *c* impact; *d* fracture cross-section

11 Typical fractured coupon appearance for TRIP780 material
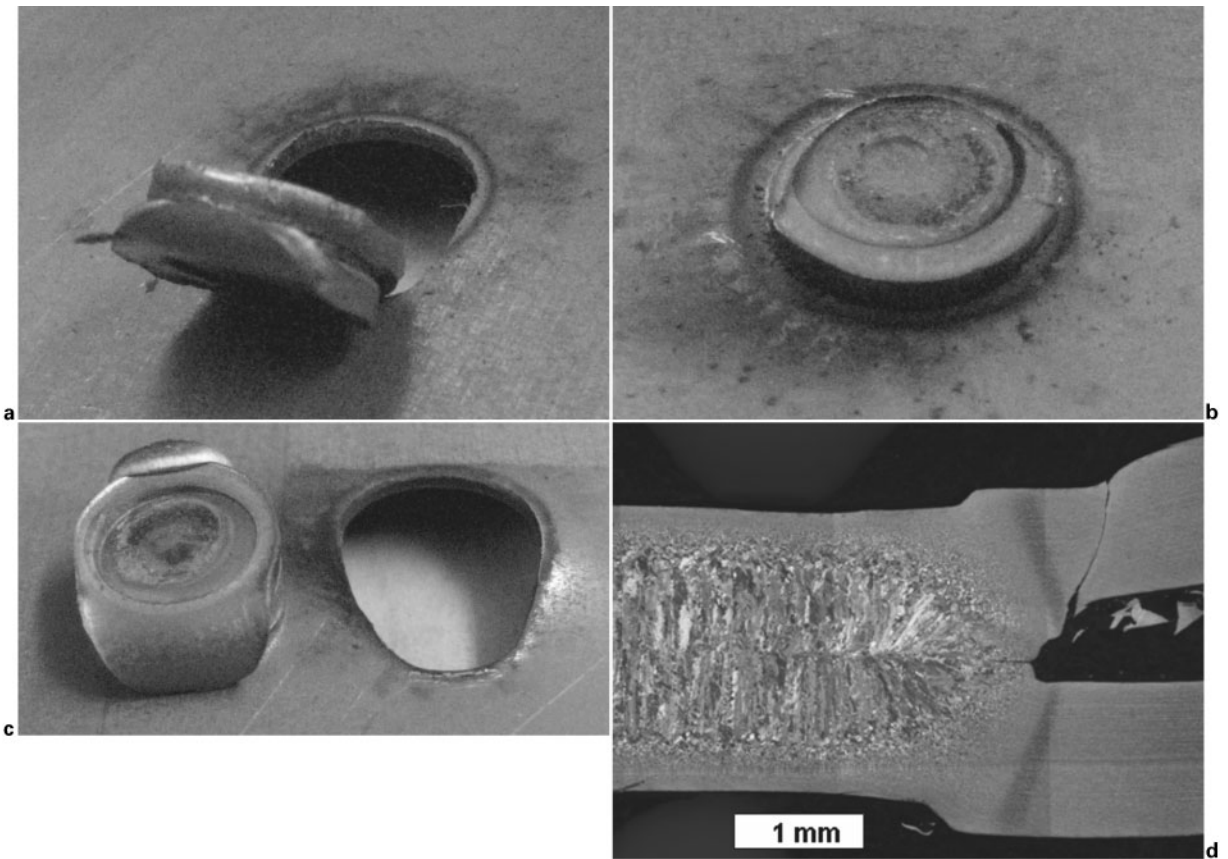
a static; *b* intermediate; *c* impact; *d* fracture cross-section

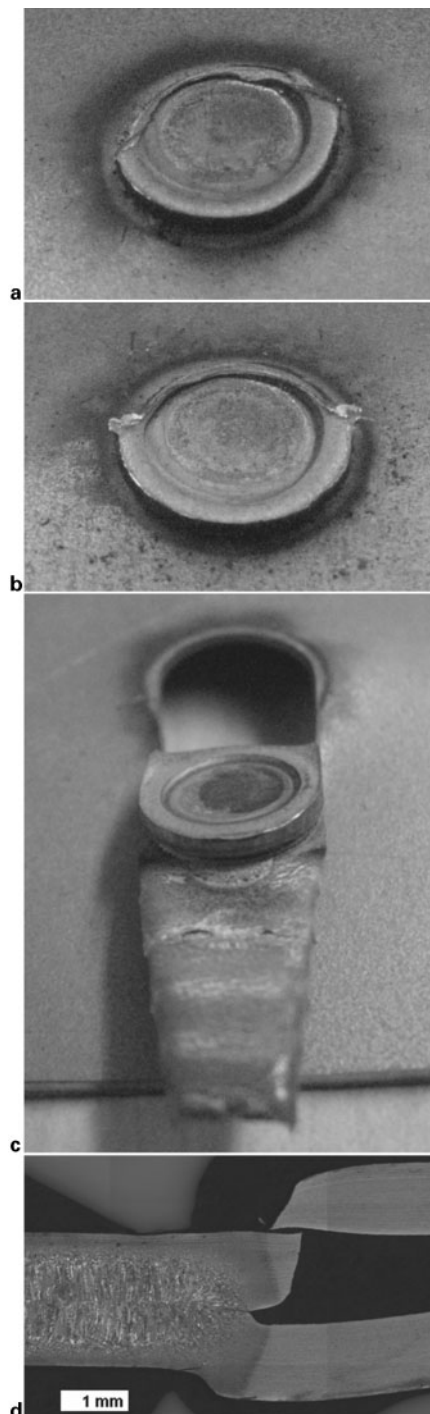**12 Typical fractured coupon appearance for DP780 material**

13 Hardness traces from base metal to fusion zone for DP780, DP600 and 590R

seen that mode C fracture occurred near the HAZ with failure propagating through the base metal. Furthermore localised necking occurs in BM of the upper sheet which indicated localised plastic deformation.

Heat affected zone softening is a noted issue when welding DP steels and has been cited for early failure.[20,21] Post weld tempering of martensite near the HAZ results in a local softened region. Materials which exhibit higher volume fractions of martensite are more susceptible to HAZ softening due to the increased volume fraction of tempered martensite after welding. As mentioned earlier, compared to the DP600, the base material of this particular DP780 contained a larger volume fraction of BM martensite. Richer chemistries coupled with increased martensite volume fraction makes the DP780 more susceptible to HAZ softening. Figure 13 shows the softened region in DP780 compared to the 590R and DP600 alloys. Furthermore, Marya *et al.*[17] examined the fracture modes for spot welded DP steels using the RSW process. In their study, increased softening in the HAZ was also reported for higher grade DP steels. The DP600 in the current study consistently produced interfacial failure resulting in reduced elongation and poor impact performance. Tensile testing of the DP780, on the other hand, consistently produced full button failure modes which followed the HAZ softened region and resulting in one of the best impact performance results. Hence, the inherent nature of DP softening, in particular for material containing higher volume fraction of martensite, can potentially aid in improving impact performance by producing ductile failure modes.

The FB 590R steel spot welds showed a failure load similar to the DP780 at impact test velocities; however, the fracture toughness at high rates was more similar to the DP600. The low energy absorption at high rates can be explained by examining the failure mode. Figure 14*a–c* shows the spot weld fracture surfaces for low, intermediate, and high test velocities, respectively. Full button pull-out failure modes during static and intermediate test velocities were observed, the failure mode is similar to the DP780. Mode D fracture initiated near the outer HAZ, in the base metal and significant base metal necking is observed in the partial tensile sample in Fig. 14*d*. The fractured spot weld for the impact

a static; *b* intermediate; *c* impact; *d* fracture cross-section
14 Typical fractured coupon appearance for 590R material

conditions shown in Fig. 14*c* reveals a unique fracture morphology. A 'comet-tail' of material was observed, showing several segments of necked base metal. This behaviour is reflected in the high rate load–displacement curve for 590R. Figure 15 illustrates the unique behaviour in which after initial fracture of the spot weld signalled by a decrease in the measured load, the load increased again up to a secondary peak, slightly lower than the initial. This cycle was repeated two times before final fracture. The comet-tail in Fig. 14*c* shows three regions of base metal necking that correspond to the peaks observed in the high rate load–displacement curve. Ferritic–bainitic steels typically have high strain hardening and high deformation. These properties
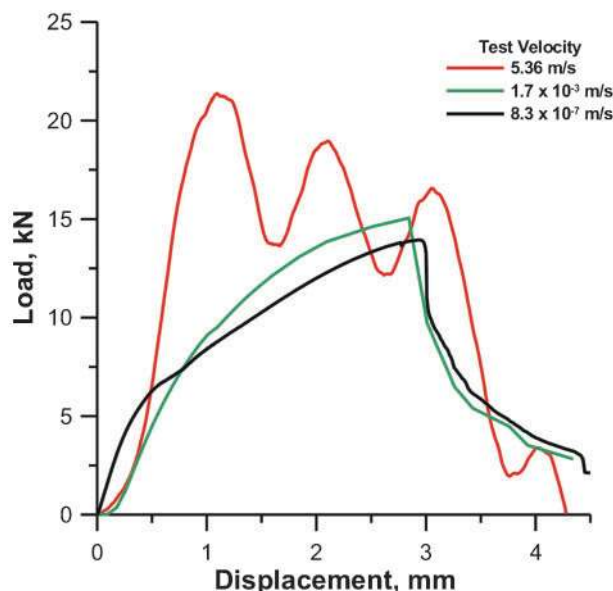
15 Load–displacement curves for 590R

explain the impact failure observations, after initial fracture around the spot weld, tearing of the base metal occurs. The comet-tail material is strain hardened preventing fracture, as shown by the secondary load increase. The cycle of tearing, and necking is repeated until final fracture occurs. The energy absorbed by the 590R spot weld continued to increase after the peak load was achieved, until final fracture occurred.

The typical method to calculate energy absorption considers only elongation until the peak load is obtained. Owing to the inherent strain hardening behaviour of the 590R, the displacement to peak load under the impact condition is quite low. Thus, the calculated impact toughness, as shown in Fig. 6, was poor compared to the other materials, such as DP780 with a similar failure load. However, it was found that after surpassing the peak load there was continued energy absorption caused by tearing of the surrounding material, given by the total area under the load–displacement curve. Calculating the total energy absorbed during impact testing of the 590R results in an increase of the normalised value from 0·49 to $\sim 2\cdot 3$ J mm^{-2}, surpassing the 1·7 J mm^{-2} absorbed by TRIP780. Therefore, it is suggested that the impact performance of the FB type 590R material is comparable to other types of AHSS. The high peak load, compared to the base metal strength is an indication of high joint efficiency, and the continued elongation after the peak load increases the total energy absorbed in a crash.

Recent work comparing the impact performance of as received HSS and AHSS can be used as a basis to compare spot weld impact performance. Oliver *et al.*[22] showed that the primarily ferritic HSLA steel exhibited the greatest increase in strength with increasing strain rate while the predominately martensitic DP material had the least strain rate sensitivity. Similarly, Fig. 4 shows the HSLA spot welds having the greatest increase in load bearing capacity transitioning from intermediate to impact test velocities while the DP780 exhibited the least increase. In a later publication by Oliver *et al.*[23] the energy absorption of TRIP and DP steel were

compared. Results showed a greater increase in energy absorption rate for the TRIP compared to the DP grades of similar strength, transitioning from static to impact test velocities; however, the DP steel consistently absorbed more energy. These results, however, do not reflect those observed in Fig. 7 where the spot welded TRIP780 exhibited the highest energy absorption compared to the DP780. Discrepancies in results may be attributed to the thermal history of spot welded material, which modifies as received strip steel microstructure typically resulting in a martensitic structure.

It should also be recognised that various processing techniques and chemistries used in AHSS production differ from manufacturers, which can also affect fracture modes. Hence, the failure modes observed in these particular AHSS may not necessarily occur in other grades, which undergo different processing techniques.

Conclusions

In the present study the fracture surfaces and impact performance of resistance spot welded AHSS were examined. A comparison was conducted by observing; failure loads, displacement, energy absorption, and fracture surfaces for static, intermediate and impact test velocities. In addition, performance results were normalised to compare relative material strength in the weld zone. The followings are key results.

1. Failure loads during tensile shear testing increased as test velocities increased; however there was no correlation between base metal strength and failure loads of the welds.

2. Four different failure modes were observed. Partial interfacial failure was observed for the TRIP780 and HSLA, where fracture propagated through the HAZ and into the FZ during intermediate test velocities. Two button pullout failure modes were obtained for 590R and DP780 for all test velocities, with failure near HAZ for DP780 and in base metal for 590R. Interfacial failure consistently occurred when testing DP600.

3. Base metal failure occurs with the 590R during static and intermediate test velocities, however tearing, was observed when subjected to impact test velocities. Tearing can improve the energy absorption of 590R spot welds if energy until fracture is calculated.

4. Heat affected zone softening observed in DP780 contributed to ductile pull-out failure modes as compared to the interfacial failure observed in the DP600, thus resulting in poor impact performance by DP600.

Acknowledgements

References

1. I. Khan, M. L. Kuntz, P. Su, A. Gerlich, T. North and Y. Zhou: *Sci. Technol. Weld. Join.*, 2007, **12**, (2), 175–182.
2. M. Kimichi: *Weld. J.*, 1984, **63**, (2), 58s–63s.
3. K. Banerjee and U. K. Chatterjee: *Metall. Mater. Trans. A*, 2003, **34A**, (6), 1297–1309.

4. S. Dinda, C. Belleau and D. K. Kelley: 'High strength low alloy steel in automotive structures', 475–483; 1984, Metals Park, OH, ASM.

5. J. Dufourny and A. Bragard: *Weld. World*, 1985, **23**, (5–6), 100–123.

6. K. W. Ewing, M. Cheresh, R. Thompson and P. Kukuchek: 'Static and impact strengths of spot-welded HSLA and low carbon steel', SAE technical paper 820281, 1982.

7. W. Peterson and F. Orth: Proc. Sheet Metal Welding Conf. XII, Livonia MI, USA, May 2006.

8. A. Pichler, S. Traint, G. Amoldner, P. Stiaszny, M. Blaimschein, E. A. Werner: Proc. 44th MWSP Conf., Vol. XL; 2002, Warrendale, PA, Iron and Steel Society.

9. 'Automotive steel design manual', Revision 6·1, AISI/ASP, August 2002.

10. 'Recommended practices for evaluating the resistance spot welding behaviour of automotive sheet steel materials', ANSI/AWS/SAE, 1997.

11. W. Tan, Y. Zhou, H. W. Kerr and S. Lawson: *J. Phys. D*, 2004, **37D**, (14), 1998–2008.

12. C. Ma, S. D. Bhole, D. L. Chen, A. Lee, E. Biro, G. Boudreau: *Sci. Technol. Weld. Join*., 2006, **11**, (4), 480–487(8).

13. H. Zhang and J. Senkara: 'Resistance welding: fundamentals and applications'; 2006, Boca Raton, FL, Taylor & Frances.

14. G. B. Frommeyer and P. Neumann: *ISIJ Int*., 2003, **43**, (3), 438–446.

15. N. D. Beynon, T. B. Jones and G. Fourlaris: *Mater. Sci. Technol.*, 2005, **21**, (1), 103–112.

16. N. D. Beynon, S. Oliver, T. B. Jones and G. Fourlaris: *Mater. Sci. Technol.*, 2005, **21**, (7), 771–778.

17. M. Marya, K. Wang, L. G. Hector and X. Gayden: *J. Manuf. Sci. Eng.*, 2006, **128**, 287–298.

18. N. Uijl and S. Smith: Proc. 4th Int. Semin. on 'Advances in resistance welding', Wels, Austria, November 2006, SWANTEC/FRONIUS, 30–62.

19. E. Girault, A. Mertens, P. Jacques, Y. Houbaert, B. Verlinden and J. V. Humbeeck: *Scr. Mater.*, 2001, **44**, 885–892.

20. E. Biro and A. Lee: Proc. SMWC XII, American Welding Society (AWS), Livonia, MI, USA, May 2006.

21. M. Xia, N. Sreenivasan, S. Lawson, Y. Zhou and Z. Tian: *J. Mater. Sci. Eng*., 2007, **129**, 446–452.

22. S. Oliver, T. B. Jones and G. Fourlaris: *Mater. Sci. Technol*., 2007, **23**, (1), 55–62.

23. S. Oliver, T. B. Jones and G. Fourlaris: *Mater. Sci. Technol*., 2007, **23**, (4), 423–431.